fishes

MDPI

Article

The Study on the Biological Characteristics of *Photobacterium damselae* subsp. *damselae* Affected by the Deletion of the Iron Uptake System Genes *tonB1* and *tonB2*

Hua Jiang [1,†], Yufei Ji [1,2,†], Zhiqi Zhang [2], Yongxiang Yu [2], Chunyuan Wang [2], Yingeng Wang [2], Xiaojun Rong [2], Aijun Ma [2], Shuyi Li [3] and Zheng Zhang [2,*]

[1] College of Food Science and Engineering, Qilu University of Technology (Shandong Academy of Sciences), Jinan 250353, China; jhmengyou@163.com (H.J.); 17398441332@163.com (Y.J.)
[2] State Key Laboratory of Mariculture Biobreeding and Sustainable Goods, Yellow Sea Fisheries Research Institute, Chinese Academy of Fishery Sciences, Qingdao 266071, China; zhangzhiqi@ysfri.ac.cn (Z.Z.); yuyx@ysfri.ac.cn (Y.Y.); wangcy@ysfri.ac.cn (C.W.); wangyg@ysfri.ac.cn (Y.W.); rongxj@ysfri.ac.cn (X.R.); maaj@ysfri.ac.cn (A.M.)
[3] Huanghua Jinhui Aquatic Products Breeding and Development Co., Ltd., Cangzhou 061102, China; jinhuishuichan@126.com
* Correspondence: zhangzheng@ysfri.ac.cn
† These authors contributed equally to this work.

Abstract

Photobacterium damselae subsp. *damselae* (PDD), a marine fish pathogen, has an unclear contribution of *tonB* genes to iron acquisition and pathogenicity. Δ*tonB1*-PDD and Δ*tonB2*-PDD mutants as well as their complemented strains were generated via homologous recombination from the virulent strain PDD1605. Growth was evaluated by monitoring OD_{600} with viable-count calibration, intracellular iron was measured using a colorimetric assay, biofilm was detected by crystal violet staining, transcription was analyzed through qRT-PCR, and pathogenicity was assessed via an 8-day intramuscular challenge in black rockfish (*Sebastes schlegelii*). Under iron limitation induced by 100 μM 2,2′-dipyridyl, the maximum density decreased from 4.51×10^8 CFU/mL in wild-type (WT-PDD) to 4.00×10^8 and 3.64×10^8 CFU/mL in Δ*tonB1*-PDD and Δ*tonB2*-PDD respectively, and was largely restored after complementation. The intracellular iron content declined from $3.75 \times 10^{-4} \pm 4.00 \times 10^{-6}$ nmol/10^6 cells in WT-PDD to $3.13 \times 10^{-4} \pm 1.05 \times 10^{-5}$ nmol/10^6 cells in Δ*tonB1*-PDD and $2.55 \times 10^{-4} \pm 2.00 \times 10^{-5}$ nmol/10^6 cells in Δ*tonB2*-PDD. Compared with WT-PDD, biofilm formation was reduced by 22.1% in Δ*tonB1*-PDD and by 24.8% in Δ*tonB2*-PDD. Deletion of *tonB2* induced mild yet statistically significant transcriptional alterations in multiple iron acquisition and virulence-related genes, while colony morphology, swarming motility, hemolysis, phospholipase activity, biochemical traits, and antimicrobial susceptibility remained unchanged. In the high-dose challenge assay, WT-PDD caused 100% mortality within 2 days, whereas Δ*tonB1*-PDD and Δ*tonB2*-PDD caused 17/20 and 18/20 deaths respectively; all infected groups reached 100% mortality by day 3. In the low-dose challenge assay, WT-PDD, Δ*tonB1*-PDD, and Δ*tonB2*-PDD caused 12/20, 12/20, and 13/20 deaths by day 2, with cumulative mortalities reaching 80%, 70%, and 80% by day 8, respectively. Kaplan–Meier analysis detected no significant differences among the survival curves at either challenge dose. These findings suggest that *tonB1* and *tonB2* play roles in iron acquisition, low-iron adaptation, and biofilm formation, with *tonB2* deletion exerting greater effects on growth and intracellular iron accumulation under iron-limited conditions.

Academic Editors: Haipeng Cao, Yibin Yang and Yali Wang

Received: 5 July 2026
Revised: 17 August 2026
Accepted: 17 August 2026
Published: 19 August 2026

Keywords: *Photobacterium damselae* subsp. *damselae*; *tonB*; iron uptake; biological characteristics; virulence genes

Key Contribution: This study demonstrates that *tonB1* and *tonB2* contribute to iron acquisition, low-iron adaptation, and biofilm formation in *Photobacterium damselae* subsp. *damselae*, with *tonB2* exerting a stronger influence on iron-dependent growth and intracellular iron accumulation.

1. Introduction

Iron is an essential micronutrient necessary for numerous biological processes, such as respiratory metabolism, DNA synthesis, and the maintenance of cellular redox homeostasis. Within vertebrate hosts, however, the availability of free iron is extremely scarce as iron is firmly sequestered by host iron-binding proteins like transferrin, lactoferrin, and heme-binding proteins. This host-mediated restriction of iron availability represents a classical defense mechanism known as nutritional immunity, which effectively restricts pathogen proliferation and colonization [1,2]. To surmount iron limitation, Gram-negative bacteria have developed a diverse array of high-affinity iron acquisition systems. Among them, the TonB-dependent transport system is one of the most extensively characterized. This system generally comprises outer membrane TonB-dependent transporters (TBDTs), the inner membrane energy-transducing complex ExbB–ExbD, and the periplasmic energy transducer TonB. ExbB and ExbD are inner membrane-associated energy-coupling proteins that utilize the proton motive force across the cytoplasmic membrane to produce the energy needed for substrate transport. TonB acts as a periplasmic energy transducer, transferring this energy across the periplasmic space to outer membrane receptors, thus enabling the uptake of siderophore–iron complexes, heme, and other substrates through the outer membrane into the periplasmic compartment [3,4]. Therefore, the TonB-dependent transport system not only functions as a core mechanism for bacterial adaptation to iron-limited environments and nutrient competition, but also serves as a critical molecular determinant for the survival, colonization, and virulence of numerous Gram-negative pathogens within their hosts [5,6].

Photobacterium damselae subsp. *damselae* (PDD), an important pathogen, is widely distributed in marine environments worldwide. It has the ability to infect a diverse range of marine cultured fish species, leading to symptoms like skin ulceration, tissue necrosis, and visceral congestion, which in turn result in high mortality rates [7–9]. Previous studies have indicated that the pathogenicity of PDD mainly relies on a set of potent toxin factors, including damselysin, HlyA-family hemolysins, and phospholipases. In addition, iron acquisition and utilization significantly impact its metabolic adaptation and virulence-associated processes [10–12]. Evidence has further demonstrated that PDD possesses multiple iron acquisition strategies, such as a heme utilization system, an iron transport mechanism mediated by secreted citrate, and a vibrioferrin-associated system [13,14]. Vibrioferrin, a low-molecular-weight siderophore originally identified in *Vibrio* species, can chelate Fe^{3+} under iron-limited conditions and promote iron acquisition and utilization through the TonB-dependent outer membrane transport system. This implies that PDD may possess strong adaptability and compensatory capacity for iron acquisition within the host environment [15,16]. Additionally, environmental factors, such as low salinity and temperature fluctuations, have been demonstrated to influence the transcriptional profile and virulence expression of this bacterium, suggesting a potential close relationship between iron metabolic adaptation and virulence regulation [17,18].

Although the importance of the TonB system has been firmly established in a wide range of Gram-negative pathogens, the number of *tonB* homologs, the extent of their functional overlap, and the degree of their association with virulence vary considerably among bacterial species. The deletion of the *tonB* gene in avian pathogenic *Escherichia coli* has been demonstrated to significantly reduce virulence. In bacteria possessing multiple TonB systems, individual homologs may exhibit both functional overlap and specialization. In the fish pathogen *Vibrio anguillarum*, two TonB systems contribute differently to iron transport and virulence [6]. Similarly, homolog-specific roles in iron-limited growth, hemin utilization, host–cell adhesion, and virulence have been reported in *Riemerella anatipestifer* and *Acinetobacter baumannii* [19–21]. These comparisons indicate that the number of TonB homologs alone does not predict their functional relationships. Of particular relevance, *tonB1* and *tonB2* were previously cloned from the closely related subspecies *Photobacterium damselae* subsp. *piscicida*. It was found that *tonB1*, but not *tonB2*, was regulated by Fur. Nevertheless, that study did not directly compare the biological roles of the two genes [22]. Evidence of a functional connection among TonB-dependent iron acquisition, biofilm formation, and virulence has been reported in other pathogens. In *Riemerella anatipestifer*, the deletion of the TonB-dependent hemin receptor gene *tbdR1* led to impairment of hemin acquisition and significantly decreased biofilm formation, adhesion to and invasion of Vero cells, and virulence in ducklings [23]. These findings indicate that TonB-dependent iron acquisition is associated with both biofilm formation and pathogenicity; however, whether a similar relationship exists in PDD remains unknown. In contrast, functional studies of *tonB* homologs in PDD are still scarce. According to the NCBI database, the PDD genome contains two *tonB* homologs, *tonB1* (Gene ID: 93397623) and *tonB2* (Gene ID: 93399754), which are located on different chromosomes and are both annotated as encoding the energy transducer TonB. This annotation suggests that at least two TonB-like energy transduction components exist in the PDD genome. However, direct experimental evidence is still absent regarding whether *tonB1* and *tonB2* make different contributions to iron acquisition, low-iron adaptation, biofilm formation, virulence-associated gene expression, and pathogenicity in PDD. Clarifying these functions is essential for a better understanding of how TonB-dependent iron uptake contributes to bacterial adaptation and infection-related phenotypes in this pathogen.

Based on the reported functional diversification of TonB homologs in other Gram-negative bacteria, we hypothesized that TonB1 and TonB2 are not fully redundant in PDD. Moreover, the deletion of either gene would differentially impact iron acquisition, adaptation to iron limitation, biofilm formation, and infection-related phenotypes. To test this hypothesis, *tonB1* and *tonB2* deletion mutants, along with their corresponding complemented strains, were constructed in the highly virulent PDD strain PDD1605. Subsequently, evaluations were carried out on growth under different iron conditions, intracellular iron accumulation, colony morphology, swarming motility, biofilm formation, hemolytic and phospholipase activities, physiological and biochemical characteristics, antimicrobial susceptibility, expression of genes related to virulence and iron uptake, and pathogenicity in black rockfish (*Sebastes schlegelii*). To our knowledge, the present study provides the initial direct comparative functional analysis of TonB1 and TonB2 in PDD. It combines gene deletion and complementation with evaluations of iron acquisition, low-iron adaptation, biofilm formation, virulence-associated phenotypes, and experimental pathogenicity.

2. Materials and Methods

2.1. Bacterial Strains and Plasmids

Photobacterium damselae subsp. *damselae* PDD1605, designated WT-PDD, was initially isolated from ulcerative black rockfish (*S. schlegelii*) cultured in marine cages and preserved

in the pathogen bank of the Yellow Sea Fisheries Research Institute, Chinese Academy of Fishery Sciences [24]. The plasmids pRE112 and pHRP309, along with *Escherichia coli* S17-1λpir, were obtained from the same institutional collection.

2.2. Construction of the ΔtonB1/ΔtonB2-PDD Deletion Mutants and C-tonB1/C-tonB2-PDD Complemented Strains

The Δ*tonB1*-PDD and Δ*tonB2*-PDD mutants were constructed via pRE112-mediated homologous recombination as previously described [25]. For the construction of Δ*tonB1*-PDD, the upstream and downstream flanking regions of *tonB1* were amplified from WT-PDD genomic DNA using the primer pairs pRE112-Δ*tonB1*-F1/R1 and pRE112-Δ*tonB1*-F2/R2, respectively. Similarly, the upstream and downstream flanking regions of *tonB2* were amplified using pRE112-Δ*tonB2*-F1/R1 and pRE112-Δ*tonB2*-F2/R2, respectively. These amplified regions were then assembled and cloned into SacI-linearized pRE112 using 2×Ezmax® Universal CloneMix (Shanghai ToloBiotech Co., Ltd., Shanghai, China). The resulting recombinant plasmids were verified by PCR using pRE112-F/R and by Sanger sequencing. Subsequently, they were introduced into *Escherichia coli* S17-1λpir and transferred into WT-PDD by biparental conjugation [26], with the donor *Escherichia coli* S17-1λpir and recipient WT-PDD cultures mixed at a volume ratio of 3:1. Single-crossover recombinants were selected on a medium containing ampicillin (100 μg/mL) and chloramphenicol (30 μg/mL), and double-crossover mutants were obtained by counterselection on TSB medium supplemented with 15% sucrose for 38 h. Candidate mutants were confirmed by PCR using in-*tonB1*-F/R or in-*tonB2*-F/R, and their genetic stability was evaluated after 50 consecutive passages.

For complementation, the *tonB1* fragment was amplified using pHRP309-*tonB1*-F/R. Two *tonB2* fragments were amplified using pHRP309-*tonB2*-F1/R1 and pHRP309-*tonB2*-F2/R2, respectively. The corresponding *tonB* fragments were amplified and cloned into EcoRI-linearized pHRP309 using 2×Ezmax® Universal CloneMix [27]. The sequence-confirmed recombinant plasmids were introduced into *E. coli* S17-1λpir and transferred into the respective deletion mutants by conjugation, with the donor *Escherichia coli* S17-1λpir and recipient deletion-mutant cultures mixed at a volume ratio of 3:1. Transconjugants were selected on medium containing ampicillin (100 μg/mL) and gentamicin (30 μg/mL), and the complemented strains C-*tonB1*-PDD and C-*tonB2*-PDD were confirmed by PCR using pHRP309-F/M13-F. All primers used in this study are listed in Table 1.

Table 1. The primers for the construction of PDD *tonB* gene mutant and complemented strains.

Primers	Sequence (5′–3′)	Product Size (bp)
pRE112-Δ*tonB1*-F1	GAATTCCCGGGAGAGCTCAAGATAATCCTAAAG ATTGGTGTTG	565
pRE112-Δ*tonB1*-R1	TCCATAATT TGTTCATAAAAGTTAAAAATAGCGA	
pRE112-Δ*tonB1*-F2	TTATGAACA AATTATGGAATTTATCAACCAATATC	
pRE112-Δ*tonB1*-R2	GCATGCGATATCGAGCTCGCCCAAAGTCCGAGC AGTT	588
in-*tonB1*-F	CTTTAAAAGCCCTTACCCA	1307 (WT-PDD)/548 (Δ*tonB1*-PDD)
in-*tonB1*-R	CTGAGCCAGATGATCCAAT	
pRE112-F	CGGGTTGAGAAGCGGTGTA	1484 (pRE112-UD-*tonB1*)
pRE112-R	CAGCCAATCCCTGGGTGAG	1289 (pRE112-UD-*tonB2*)
pHRP309-*tonB1*-F	GGTACCGAGCTCGAATTCAAGATAATCCTAAAG ATTGGTGTTG	1537
pHRP309-*tonB1*-R	GAGGATCCCCGGGAATTCTTAATCCAATTGAAA ACGTACAGG	

Table 1. *Cont.*

Primers	Sequence (5′–3′)	Product Size (bp)
pRE112-Δ*tonB2*-F1	GAATTCCCGGGAGAGCTCAAGATAATCCTAAAG ATTGGTGTTG	375
pRE112-Δ*tonB2*-R1	CTTCATCAT CCTACTCCCCTAACCATCACTTATT GGGAGTAGG	
pRE112-Δ*tonB2*-F2	ATGATGAAGATAAAAAAGCCATTAG GCATGCGAATATCGAGCTCCCTAGAGCAATAGA AAGTGGTGACA	584
pRE112-Δ*tonB2*-R2		
in-*tonB2*-F	GGATGCCTCCTTGGTTAT	1013 (WT-PDD)/356(Δ*tonB2*-PDD)
in-*tonB2*-R	TTGCAGATTGGGCTTTAC	
pHRP309-*tonB2*-F1	GGTACCGAGCTCGAATTCACGCTTAGCTTTACGT CTTACTTGA	1041
pHRP309-*tonB2*-R1	TCTTAACAT CTGATGACCTAATAAAGCAACGT GGTCATCAG	
pHRP309-*tonB2*-F2	ATGTTAAGAGTCTTAATGGCTTTTC GAGGATCCCCGGGAATTCTCATTGATTTATTTTA AACTCCAAT	684
pHRP309-*tonB2*-R2		
pHRP309-F	ACTGATGGCGCCGTGTT	1827 (C-*tonB1*-PDD)
M13-F	TGTAAAACGACGGCCAGT	2101 (C-*tonB2*-PDD)

2.3. Colony Morphology Observation

WT-PDD, Δ*tonB1*-PDD, and Δ*tonB2*-PDD strains were streaked onto TSB, 2216E, TCBS, and LB agar media containing 1.5% NaCl, either with or without 50 or 75 μM 2,2′-dipyridyl (dip). After incubation at 28 °C for 24 h, the colony morphology was recorded [28,29].

2.4. Growth Curve Analysis and Determination of Iron Uptake Capacity of WT-PDD, ΔtonB1/ΔtonB2-PDD, and C-tonB1/C-tonB2-PDD Under Different Iron Conditions

Growth was evaluated in 96-well liquid cultures under different iron-availability conditions, following the general microplate-based strategy used for iron-related growth assays in fish-pathogenic *Vibrionaceae* [30]. WT-PDD, Δ*tonB1*-PDD, and Δ*tonB2*-PDD were cultured in LB broth containing 1.5% NaCl, LB broth containing 1.5% NaCl plus 100 μM dip, or LB broth containing 1.5% NaCl plus 10 μM $Fe_2(SO_4)_3$. C-*tonB1*-PDD and C-*tonB2*-PDD were examined only under the 100 μM dip condition. Overnight cultures were diluted at a ratio of 1:50 into the corresponding fresh media, and 200 μL aliquots were inoculated into sterile 96-well plates. Uninoculated medium served as the blank control. The OD_{600} was recorded every 2 h using an automated growth curve analyzer (Bioscreen C Pro, Oy Growth Curves Ab Ltd., Turku, Finland). Viable counts corresponding to different OD_{600} values were determined by serial dilution plating to establish an OD_{600}–CFU regression curve for WT-PDD. This experiment was replicated three times.

Intracellular iron content was measured under iron-limited conditions. WT-PDD, Δ*tonB1*-PDD, Δ*tonB2*-PDD, C-*tonB1*-PDD, and C-*tonB2*-PDD were cultured in LB broth containing 1.5% NaCl and 100 μM dip, then diluted 1:100 into fresh medium, and incubated until the OD_{600} reached approximately 1.0. Cells from a 1 mL culture were harvested, washed twice with sterile 0.9% saline, and analyzed using a Total Cellular Iron Colorimetric Assay Kit (Wuhan Elabscience Biotechnology Co., Ltd., Wuhan, China) according to the manufacturer's instructions. The iron content was normalized to the number of bacterial cells, and each strain was tested in triplicate. This experiment was replicated three times.

2.5. Swarming Motility Assay

WT-PDD, Δ*tonB1*-PDD, Δ*tonB2*-PDD, C-*tonB1*-PDD, and C-*tonB2*-PDD were cultured in TSB broth at 28 °C until the OD_{600} reached approximately 0.6. Then, 3 μL aliquots were spotted onto the surface of semisolid TSB medium containing 0.6% agar. After a 24 h incubation at 28 °C, the diameters of the motility zones were measured. Five replicate plates were used for each strain. This experiment was replicated three times.

2.6. Effects of tonB Gene Deletion on the Expression of Genes Related to Virulence and Iron Uptake, and Virulence-Related Phenotypes of PDD

WT-PDD, Δ*tonB1*-PDD, and Δ*tonB2*-PDD were cultured overnight at 28 °C in LB broth containing 1.5% NaCl. Total RNA was extracted using an RNA Extraction Kit (Vazyme Biotech Co., Ltd., Nanjing, China) and reverse-transcribed into cDNA using a reverse transcription kit (Vazyme Biotech Co., Ltd., Nanjing, China), following the manufacturer's instructions. RT-qPCR was performed to analyze the expression of genes related to virulence (*dly*, $hlyA_{ch}$, $hlyA_{pl}$, and *plpV*), iron uptake (*tonB1*, *tonB2*, *fur*, *cyaY*, and *hutZ*), outer membrane (*flhB* and *ompP*), the lipopolysaccharide-associated (*lapB*), chemotaxis (*cheW* and *cheY*), and the flagellar (*flgK*). *gyrB* was employed as the internal reference gene. Primers were designed based on the WT-PDD genome sequence (NCBI accession no. NZ_CP073684.1) and are listed in Table 2. Amplification was performed at 95 °C for 30 s, followed by 40 cycles of 95 °C for 10 s and 60 °C for 30 s. Relative expression levels were calculated using the $2^{-\Delta\Delta Ct}$ method [31], and each assay was performed in triplicate. This experiment was replicated three times.

Table 2. The primers for qRT-PCR analysis of PDD virulence-related genes.

Genes	Sequence (5′-3′)	Fragment Size (bp)	Genes	Sequence (5′-3′)	Fragment Size (bp)
gyrB	F: GTGATACTGATCGTACAGGT R: CTTTCTGGTGAATTGGTGTT	246	*cyaY*	F:ATTAACCGCCAAGAACCGCT R:CCGATTCGCCAGCATGTAGA	157
hutZ	F:TTCTGCGATGCCCTTCTGTT R:GCTCAGCGGCTTAGAGGATT	140	*tonB1*	F:ATGGCTGTTAATGCCGCTTG R:ACCCAAGATTGGCAAAACGC	142
tonB2	F:CAGTGCTCGCATTGCATCTC R:AACCTCGTTATCCAGCACGG	152	*dly*	F: ATGCGACAGCACAAGAACC R: GACCGCTCGTCCAAATAAG	236
plpV	F: AACGCTGCTGATATTACCTA R: GCCTAAGAACCAAGAGTTTG	195	$hlyA_{pl}$	F: AAAACTCGCATAACTAAGAGG R: GTAAAGATGGACCGAAAGC	248
$hlyA_{ch}$	F: GATAACCTTCCGACCATACA R: CGAGTCTTCAGGCTAATGC	186	*fur*	F: CACATTAGTGCGGAAGACC R: TTGCCACAATCTAAACAAACA	197
cheW	F: AGAGGCTAAATGGGTTGAC R: TCCTGATTCTAAGGGGTCTA	139	*cheY*	F: GTCGGTAATAACAAAGTCAAA R: GTGAAGAACTTACTGCGTGA	111
ompP	F: CACTGGTAACTTTGGTGGTC R: GGTGTAGTACCTTGCTGATTT	174	*lapB*	F: ATGATTGAGTTAGGTGCCC R: TTGCCTGCTTGTATTCTTG	139
flhB	F: TCAGGCTTACCTTCTGTCTC R: CTGCTCGTTATTAGTGGTTG	123	*flgK*	F: GTTTGTTTCGCTTGTTCTAA R: CGATAATGTTTCTCGTGCT	240

Hemolytic and phospholipase activities were examined using agar well-diffusion assays. LB agar containing 1.5% NaCl, with no addition, 100 μM dip, or 10 μM $Fe_2(SO_4)_3$, was supplemented with either 5% defibrinated sheep blood or 3% egg yolk emulsion. Aliquots of 200 μL bacterial culture were added to each well, and the plates were incubated at 28 °C for 48 h. Sterile LB broth containing 1.5% NaCl was used as the negative control. Hemolytic zones and phospholipase halos were recorded, and all assays were performed in triplicate. This experiment was replicated three times.

2.7. Biofilm Formation Assay

Biofilm formation was quantitatively measured using the crystal violet microtiter plate assay [32,33]. WT-PDD, Δ*tonB1*-PDD, and Δ*tonB2*-PDD were cultured in TSB broth at

28 °C until the OD_{600} reached 0.5–0.6, and then they were diluted 100-fold. Subsequently, 200 µL aliquots of the diluted cultures were added to sterile 96-well plates, with sterile TSB serving as the negative control. After incubation at 28 °C for 48 h, the planktonic cells were removed, and the wells were washed with sterile PBS. The attached biofilms were fixed with methanol for 15 min, stained with crystal violet for 5 min, washed, and then dissolved in 100 µL of 95% ethanol. The biofilm biomass was determined by measuring the absorbance at 595 nm. Five replicate wells were used for each strain. This experiment was replicated three times.

2.8. Physiological and Biochemical Characterization

Physiological and biochemical characteristics of WT-PDD, Δ*tonB1*-PDD, and Δ*tonB2*-PDD were examined using commercial micro-biochemical identification tubes (Qingdao Hope Bio-Technology Co., Ltd., Qingdao, China) following the manufacturer's instructions. The inoculated tubes were incubated at 28 °C for 48 h, and three replicates were prepared for each strain. This experiment was replicated three times.

2.9. Antimicrobial Susceptibility Testing

Antimicrobial susceptibility was evaluated using a modified disk diffusion assay in accordance with CLSI VET03 [34]. Bacterial suspensions were adjusted to an OD_{600} of approximately 0.4 with sterile 1.5% NaCl, and 100 µL aliquots were evenly spread onto TSB agar plates. Antibiotic disks were carefully placed on the inoculated plates, which were then incubated at 28 °C for 48 h. Inhibition zone diameters were measured and used to compare antimicrobial susceptibility profiles among WT-PDD, Δ*tonB1*-PDD, and Δ*tonB2*-PDD. Three replicates were performed for each strain. This experiment was replicated three times.

2.10. Comparison of Pathogenicity Between WT-PDD and ΔtonB1/ΔtonB2-PDD

The pathogenicity of WT-PDD, Δ*tonB1*-PDD, and Δ*tonB2*-PDD was evaluated by means of an intramuscular challenge assay in black rockfish (*S. schlegelii*), referring to injection-based fish virulence assays of PDD mutants [35]. The experiment was conducted in the Aquarium Laboratory of Yellow Sea Fisheries Research Institute, Chinese Academy of Fishery Sciences. Black rockfish with an average body length of 11 ± 1 cm and a mean body weight of 26 ± 2 g were acclimatized for one week at a temperature of 22 ± 2 °C during which they were fed a commercial floating pelleted diet. One-third of the water volume in each rearing system was renewed daily, and the fish were subjected to a 24-h fasting period before the challenge. Briefly, each strain was cultured in TSB broth at 28 °C with shaking at 180 rpm for 12 h. Subsequently, it was transferred at a ratio of 1:100 into fresh TSB broth and incubated for another 12 h. Bacterial cells were harvested through centrifugation, washed, and resuspended in sterile 0.9% saline. Suspensions were adjusted to 10^8 and 10^6 CFU/mL, and the actual bacterial concentrations were verified by serial dilution plating. For each dose, 20 fish were intramuscularly injected with 100 µL of bacterial suspension. Control fish were injected with 100 µL of sterile 0.9% saline. Mortality was recorded for 8 days, and pathogenicity was assessed by comparing survival rates among the different challenge groups.

2.11. Statistical Analysis

Statistical analyses were performed using SPSS v.16.0, Origin 2021, and GraphPad Prism 10.1.2. Data are presented as the mean ± standard deviation (SD). Differences among multiple groups were analyzed via one-way analysis of variance (one-way ANOVA), followed by Tukey's post hoc multiple-comparison test. The OD_{600} values of the growth curve were analyzed using two-way repeated-measures ANOVA with strain and

time as factors. Subsequently, Tukey's multiple-comparisons test was conducted among strains at each time point. Kaplan–Meier survival curves were separately compared at each challenge dose by using the log-rank (Mantel–Cox) test with Bonferroni-adjusted pairwise comparisons; $p < 0.05$ was regarded as statistically significant.

3. Results

3.1. Construction of the ΔtonB1/ΔtonB2-PDD Deletion Mutants and C-tonB1/C-tonB2-PDD Complemented Strains

Using the genomic DNA of WT-PDD as the template, specific primer pairs *tonB1/2*-1F/*tonB1/2*-1R (Sac I) and *tonB1/2*-2F/*tonB1/2*-2R (Sac I) were used to amplify fragments. The amplified fragments were then ligated into plasmid pRE112, and the resulting recombinant plasmids were transformed into competent *E. coli* S17-1λpir cells. The *tonB1* and *tonB2* deletion mutants generated by homologous recombination were serially passaged for 50 generations. Subsequently, genomic DNA was extracted and subjected to PCR verification with the primer pairs in-*tonB1/2*-F and in-*tonB1/2*-R. The anticipated amplicon sizes for the *tonB1* region were 1307 bp in WT-PDD and 548 bp in Δ*tonB1*-PDD. In contrast, for the *tonB2* region, the expected sizes were 1013 bp in WT-PDD and 356 bp in Δ*tonB2*-PDD. Agarose gel electrophoresis of the PCR products showed bands whose migration positions were consistent with the respective expected sizes. These results indicated that the constructed *tonB1* and *tonB2* deletion mutants possessed good genetic stability and homogeneous genetic characteristics (Figure 1A).

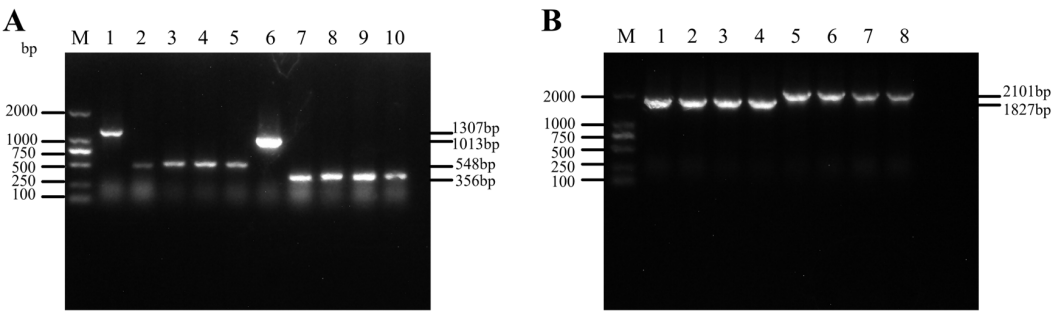

Figure 1. Construction and verification of the Δ*tonB1*/Δ*tonB2*-PDD deletion mutant and the complemented strain C-*tonB1*/C-*tonB2*-PDD. (**A**): The PCR detection results after 50 consecutive passages. Lane M represents the DL2000 DNA marker. Lane 1 shows the verification of WT-PDD using the in-*tonB1*-F and in-*tonB1*-R primers. Lanes 2–5 display the stably passaged Δ*tonB1*-PDD mutant strain. Lane 6 presents the verification of WT-PDD with the in-*tonB2*-F and in-*tonB2*-R primers. Lanes 7–10 exhibit the stably passaged Δ*tonB2*-PDD mutant strain. (**B**): Construction and verification of the complemented strain C-*tonB1*/C-*tonB2*-PDD. Lane M is the DL2000 DNA marker. Lanes 1–4 are the C-*tonB1*-PDD complemented strains, and lanes 5–8 are the C-*tonB2*-PDD complemented strains.

To generate the complemented strains, the *tonB1* and *tonB2* gene sequences were amplified and cloned into plasmid pHRP309 following the same procedure as described above. The resulting recombinant plasmids were then transformed into competent *E. coli* S17-1λpir cells. After verification, positive *E. coli* transformants were conjugated with the corresponding *tonB1* or *tonB2* deletion mutants. After selection on media containing ampicillin (Amp) and gentamicin (Gm), complemented strains carrying the recombinant vectors were obtained. PCR amplification using the primers pHRP309-F and M13-F was expected to yield amplicons of 1827 bp for C-*tonB1*-PDD and 2101 bp for C-*tonB2*-PDD. Agarose gel electrophoresis of the PCR products showed bands whose migration positions were consistent with the respective expected sizes (Figure 1B).

3.2. Morphological Characteristics

After streak cultivation on TSB agar, 2216E agar, TCBS agar, and iron-restricted LB agar media for 24 h, no obvious differences in colony morphology were observed among WT-PDD, Δ*tonB1*-PDD, and Δ*tonB2*-PDD (Figure 2). Colonies grown on TSB agar, 2216E agar, and iron-restricted LB agar were pale yellow and opaque. In contrast, colonies grown on TCBS agar were green, semi-transparent, had smooth edges, and had a flat-circular appearance. These observations indicated that the deletion of *tonB1* or *tonB2* had no apparent impact on the colony morphology of PDD. Although bacterial growth was moderately constrained under low-iron conditions supplemented with 75 μM 2,2′-dipyridyl (dip), no obvious morphological differences were noted between WT-PDD and the Δ*tonB1*-PDD or Δ*tonB2*-PDD mutants.

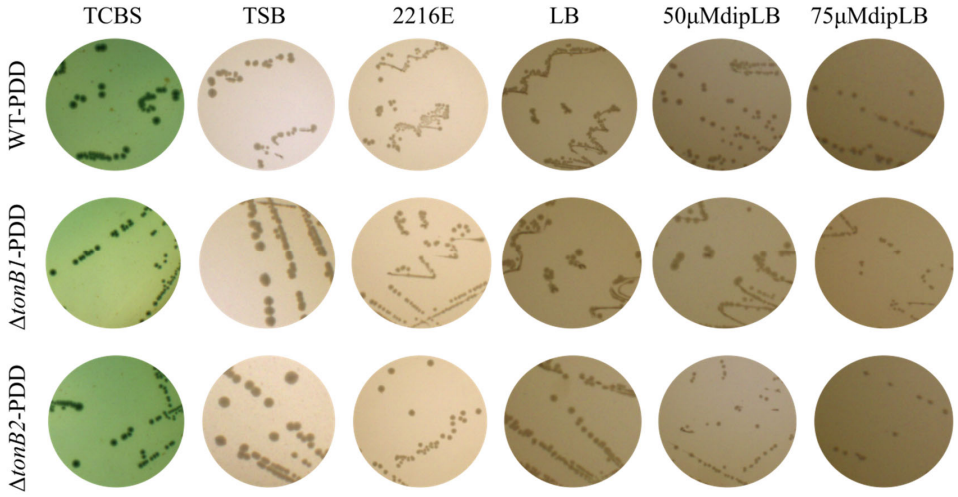

Figure 2. Comparison of colony morphology between WT-PDD and Δ*tonB1*/Δ*tonB2*-PDD.

3.3. Growth Performance and Iron Uptake Capacity of WT-PDD and ΔtonB1/ΔtonB2-PDD Under Different Iron Conditions

Under normal iron conditions (where the total iron concentration in LB broth is approximately 4–10 μM [36]), WT-PDD, Δ*tonB1*-PDD, and Δ*tonB2*-PDD rapidly entered the exponential growth phase within the first 4 h of incubation. WT-PDD reached a peak bacterial density of approximately 5.09×10^8 CFU/mL at around 18 h, corresponding to an OD_{600} value of 0.70 ± 0.01. The growth patterns of Δ*tonB1*-PDD and Δ*tonB2*-PDD were generally similar, with peak bacterial densities of approximately 4.58×10^8 and 4.66×10^8 CFU/mL, respectively, corresponding to OD_{600} values of 0.63 ± 0.02 and 0.64 ± 0.01. Overall, the growth capacities of Δ*tonB1*-PDD and Δ*tonB2*-PDD were slightly lower than that of WT-PDD under normal iron conditions ($p < 0.05$) (Figure 3A,D).

Under low-iron conditions (where the available iron is approximately 0–0.2 μM), WT-PDD, Δ*tonB1*-PDD, and Δ*tonB2*-PDD exhibited slow growth during the first 4 h, with no substantial increase in bacterial density observed. All three strains entered the exponential growth phase between 4 and 8 h. WT-PDD reached a peak bacterial density of approximately 4.51×10^8 CFU/mL at 14 h, corresponding to an OD_{600} value of 0.62 ± 0.02. In comparison, the peak bacterial densities of Δ*tonB1*-PDD and Δ*tonB2*-PDD were approximately 4.00×10^8 CFU/mL and 3.64×10^8 CFU/mL, respectively, corresponding to OD_{600} values of 0.55 ± 0.01 and 0.50 ± 0.01. WT-PDD exhibited a greater growth capacity than either deletion mutant ($p < 0.05$). In addition, the growth capacity of Δ*tonB2*-PDD was significantly lower than that of Δ*tonB1*-PDD ($p < 0.05$) (Figure 3B,D). The growth capacities of both complemented strains were substantially restored to the level of the wild-type strain WT-PDD.

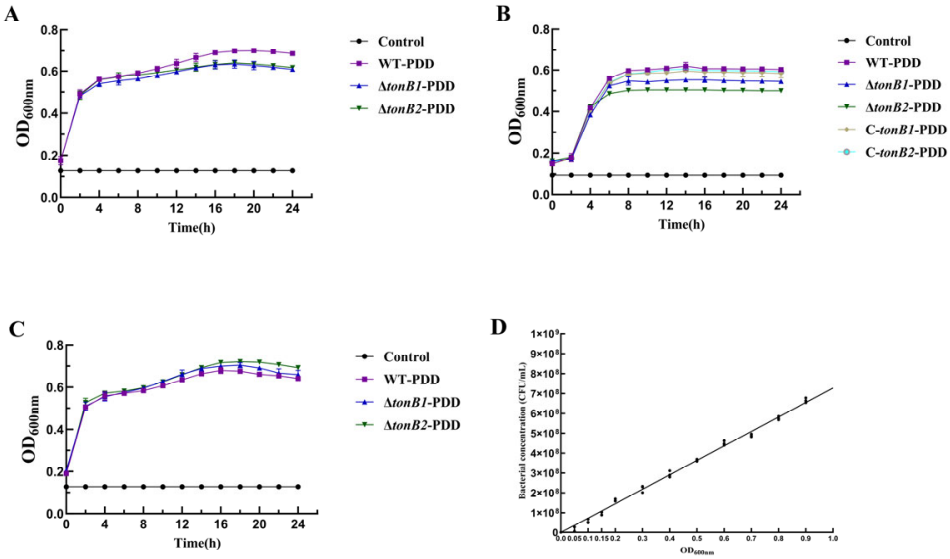

Figure 3. Comparison of growth performance between WT-PDD and Δ*tonB1*/Δ*tonB2*-PDD. The optical density at 600 nm (OD_{600}) was measured at each time point using a spectrophotometer. The results were presented as the mean ± standard deviation (n = 3). (**A**): Growth of WT-PDD and Δ*tonB1*/Δ*tonB2*-PDD under normal iron conditions. (**B**): Growth of WT-PDD, Δ*tonB1*/Δ*tonB2*-PDD, and C-*tonB1*/C-*tonB2*-PDD under low-iron conditions (100 μM dip). (**C**): Growth of WT-PDD and Δ*tonB1*/Δ*tonB2*-PDD under high-iron conditions (10 μM $Fe_2(SO_4)_3$). (**D**): Linear regression curve of OD_{600nm} versus viable bacterial concentration of WT-PDD. $y = 7.276 \times 10^8 x$ (uncentered $R^2 = 0.9980$), x: OD_{600nm}, y: bacterial concentration (CFU/mL).

Under high-iron conditions (with a total iron concentration of approximately 24.3–29.6 μM), WT-PDD reached a peak bacterial density of approximately 4.95×10^8 CFU/mL at 18 h, corresponding to an OD_{600} value of 0.68 ± 0.01. The peak bacterial densities of Δ*tonB1*-PDD and Δ*tonB2*-PDD were approximately 5.09×10^8 CFU/mL and 5.24×10^8 CFU/mL, respectively, corresponding to OD_{600} values of 0.70 ± 0.01 and 0.72 ± 0.01. Overall, the growth capacity of Δ*tonB2*-PDD was slightly higher than that of WT-PDD under high-iron conditions ($p < 0.05$) (Figure 3C,D).

The intracellular total iron content, determined by the Total Cellular Iron Colorimetric Assay Kit, indicated that under low-iron conditions, WT-PDD had an intracellular total iron content of $3.75 \times 10^{-4} \pm 4 \times 10^{-6}$ nmol/10^6 cells. In comparison, the intracellular iron content of Δ*tonB1*-PDD was $3.13 \times 10^{-4} \pm 1.05 \times 10^{-5}$ nmol/10^6 cells, significantly lower than that of WT-PDD ($p < 0.01$). The intracellular iron content of Δ*tonB2*-PDD was $2.55 \times 10^{-4} \pm 2 \times 10^{-5}$ nmol/10^6 cells, markedly lower than that of WT-PDD ($p < 0.0001$). Moreover, the intracellular total iron content of Δ*tonB2*-PDD was significantly lower than that of Δ*tonB1*-PDD ($p < 0.01$). In both complemented strains, the intracellular total iron content was largely restored to the level observed in WT-PDD (Figure 4).

These results indicated that deletion of *tonB1 and tonB2* had an impact on the growth capacity of PDD, and the magnitude of this effect varied under different iron conditions. Under normal iron conditions, the deletion of *tonB1* or *tonB2* exerted minimal influence on bacterial growth. Under low-iron conditions, the growth of the Δ*tonB2*-PDD mutant was more markedly impaired and consistently lower than that of WT-PDD. In contrast, under high-iron conditions, the deletion of *tonB2* had only a marginal effect on bacterial growth. Furthermore, the deletion of either *tonB1* or *tonB2* decreased the iron uptake capacity of PDD under low-iron conditions, with the effect of *tonB2* deletion being more pronounced than that of *tonB1* deletion.

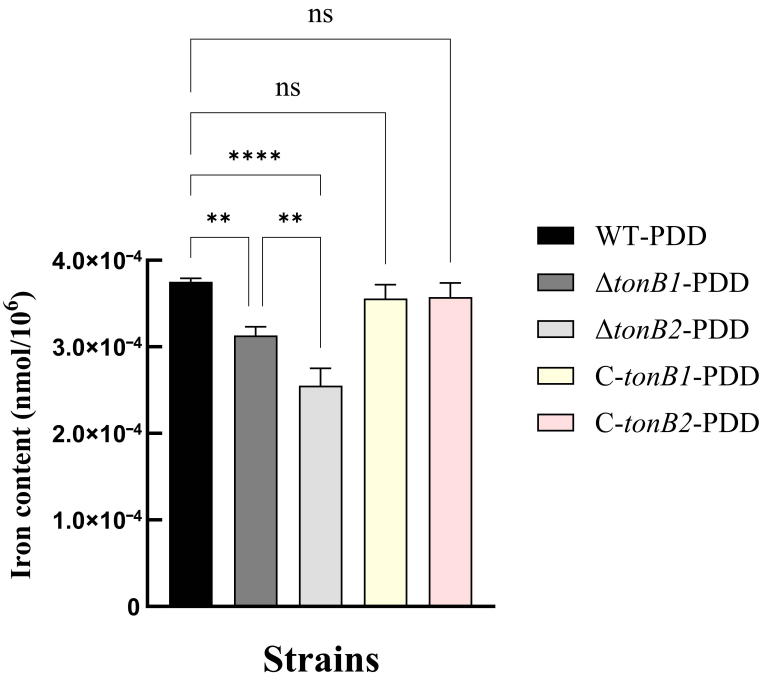

Figure 4. Comparison of the intracellular total iron content between WT-PDD, Δ*tonB1*/Δ*tonB2*-PDD, and C-*tonB1*/C-*tonB2*-PDD under low-iron conditions. The results were presented as the mean ± standard deviation (n = 3). ns indicates no significant difference ($p \geq 0.05$); ** indicates a significant difference ($p < 0.01$); **** indicates an extremely significant difference ($p < 0.0001$).

3.4. Effect of tonB1/tonB2 Deletion on the Swarming Motility of PDD

After incubation on semisolid TSB medium containing 0.6% agar at 28 °C for 24 h, the swarming motility of WT-PDD, Δ*tonB1*-PDD, Δ*tonB2*-PDD, C-*tonB1*-PDD, and C-*tonB2*-PDD was evaluated by measuring the diameters of the swarming zones. The swarming zone diameters of the wild-type strain, deletion mutants, and complemented strains were all 13 ± 0.76 mm, and no significant differences were detected among the strains (Figure 5). These results indicated that the deletion of *tonB1* or *tonB2* had no significant impact on the swarming motility of PDD.

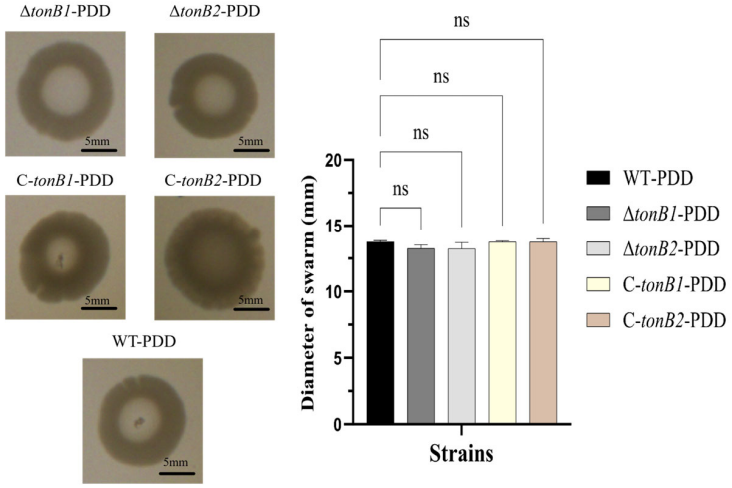

Figure 5. Swarming motility analysis of WT-PDD, Δ*tonB1*/Δ*tonB2*-PDD, and C-*tonB1*/C-*tonB2*-PDD. The results were presented as the mean ± standard deviation (n = 3). ns indicates no significant difference ($p \geq 0.05$).

3.5. Effects of tonB Deletion on Virulence Gene Expression and Virulence-Related Phenotypes of PDD

The relative expression levels of virulence-related genes, iron acquisition-related genes, and flagellum-associated genes were analyzed via qRT-PCR in WT-PDD, Δ*tonB1*-PDD, and Δ*tonB2*-PDD. As shown in Figure 6, there were no significant changes in the expression levels of the analyzed genes in Δ*tonB1*-PDD when compared with WT-PDD. Conversely, Δ*tonB2*-PDD exhibited statistically significant yet modest changes in the expression of several genes. The heme utilization-related gene *hutZ*, virulence genes $hlyA_{pl}$, $hlyA_{ch}$, and *plpV*, lipopolysaccharide-associated gene *lapB*, and iron uptake regulatory gene *fur* were all significantly upregulated ($p < 0.01$). In addition, the iron acquisition-related gene *tonB1* (encoding the TonB energy transducer), the virulence gene *dly*, and the chemotaxis-related gene *cheY* were significantly upregulated ($p < 0.05$). No significant changes were detected in the expression levels of the remaining genes (Figure 6).

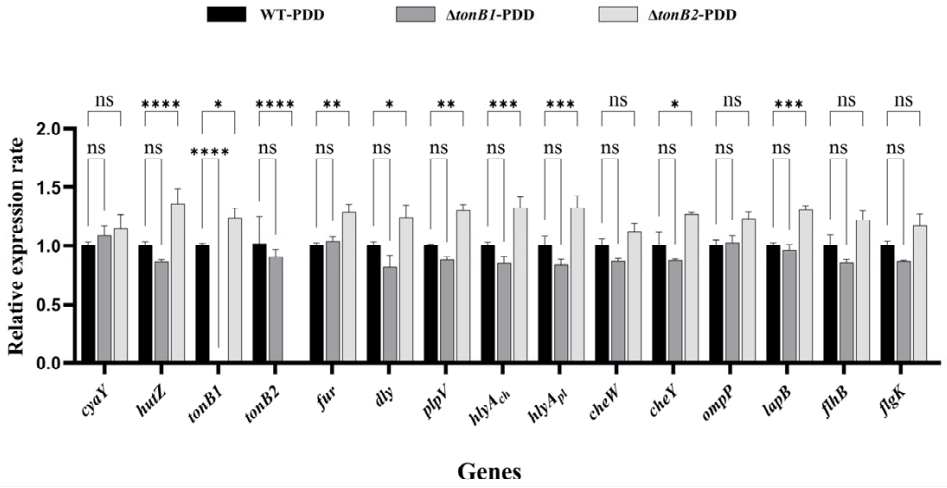

Figure 6. Relative expression levels analysis of virulence, iron uptake system, outer membrane, and flagellum-related genes in WT-PDD and Δ*tonB1*/Δ*tonB2*-PDD. The results were presented as the mean ± standard deviation ($n = 3$). ns indicates no significant difference ($p \geq 0.05$); * indicates a statistically significant difference ($p < 0.05$); ** indicates a significant difference ($p < 0.01$); *** indicates a highly significant difference ($p < 0.001$); **** indicates an extremely significant difference ($p < 0.0001$).

As shown in Figure 7A, WT-PDD, Δ*tonB1*-PDD, and Δ*tonB2*-PDD all exhibited positive β-hemolytic activity under diverse iron conditions, namely normal iron conditions, low-iron conditions (100 μM dip), and high-iron conditions (10 μM $Fe_2(SO_4)_3$). Under normal- and high-iron conditions, the diameters of the hemolytic zones produced by WT-PDD, Δ*tonB1*-PDD, and Δ*tonB2*-PDD were uniformly 7.18 ± 0.23 mm. Under low-iron conditions, the diameters of the hemolytic zones produced by all three strains were 6.31 ± 0.15 mm. As shown in Figure 7B, under normal- and high-iron conditions, WT-PDD, Δ*tonB1*-PDD, and Δ*tonB2*-PDD formed translucent halos with diameters of 11.83 ± 0.65 mm on egg yolk agar plates. Under low-iron conditions, the diameters of the translucent halos produced by all three strains were 10.02 ± 0.33 mm. These findings indicated that deletion of *tonB1* or *tonB2* did not impact the hemolytic activity or phospholipase activity of PDD.

3.6. Comparison of Biofilm Formation Ability

The biofilm-forming capabilities of WT-PDD, Δ*tonB1*-PDD, and Δ*tonB2*-PDD were evaluated via the crystal violet microtiter plate assay. As shown in Figure 8, the OD_{595} values of WT-PDD, Δ*tonB1*-PDD, and Δ*tonB2*-PDD were 1.49 ± 0.10, 1.16 ± 0.05, and 1.12 ± 0.04, respectively. In comparison with WT-PDD, the biofilm-forming capabilities of Δ*tonB1*-PDD and Δ*tonB2*-PDD were reduced by 22.1% and 24.8%, respectively. These

results suggest that *tonB1* and *tonB2* might participate in the regulation of biofilm formation in PDD. The diminished biofilm formation in both *tonB* mutants indicates that *tonB1* and *tonB2* play a role in biofilm-associated surface colonization in PDD.

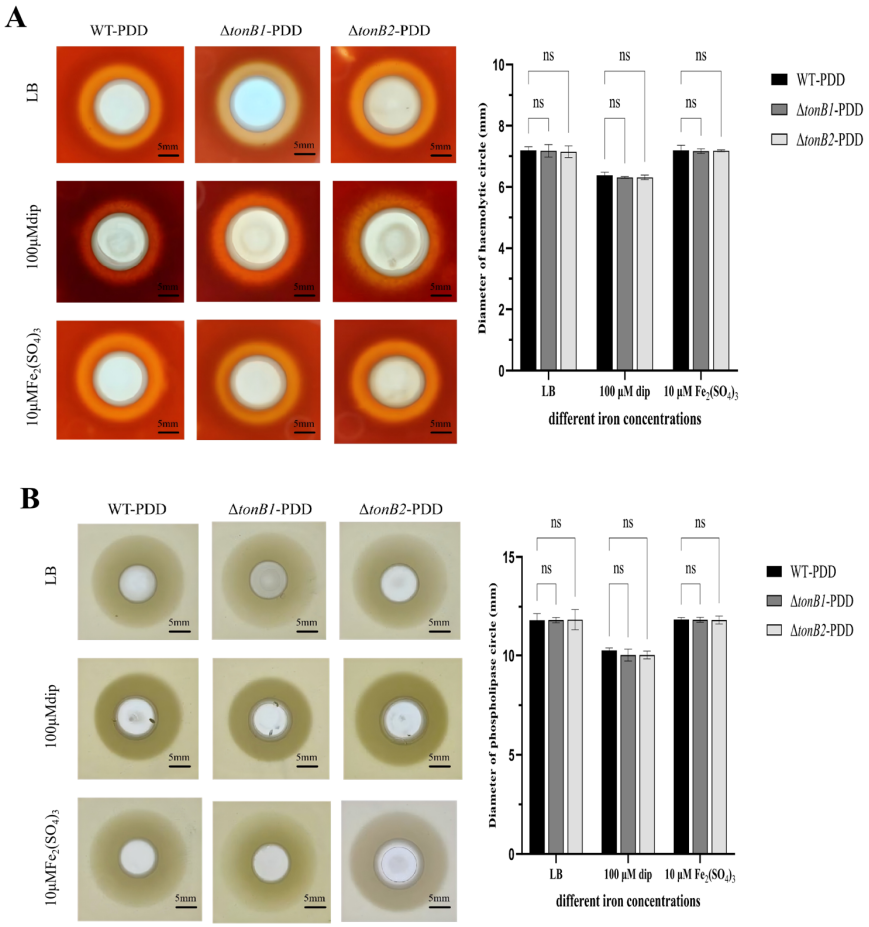

Figure 7. Hemolytic activity and phospholipase activity of WT-PDD and Δ*tonB1*/Δ*tonB2*-PDD under different iron concentrations. The results were presented as the mean ± standard deviation ($n = 3$). ns indicates no significant difference ($p \geq 0.05$). (**A**): Hemolytic zone diameters of WT-PDD and Δ*tonB1*/Δ*tonB2*-PDD under different iron conditions on perforated sheep blood agar plates, along with the statistical analysis of hemolytic zone diameters. (**B**): Phospholipase activity halos of WT-PDD and Δ*tonB1*/Δ*tonB2*-PDD under different iron conditions on perforated egg yolk agar plates, along with the statistical analysis of halo diameters.

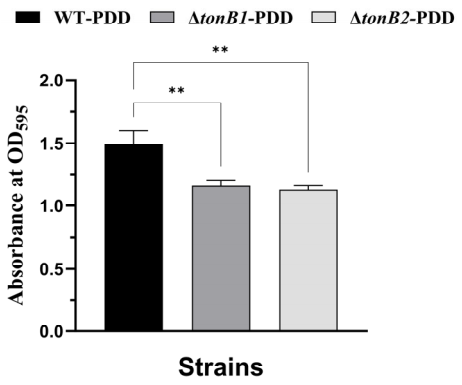

Figure 8. Comparison of the biofilm-forming ability between WT-PDD and Δ*tonB1*/Δ*tonB2*-PDD. The biofilm-forming ability was expressed as OD_{595}. The results were presented as the mean ± standard deviation ($n = 3$). ** indicates a significant difference ($p < 0.01$).

3.7. Analysis of Physiological and Biochemical Characteristics

The physiological and biochemical characteristics of WT-PDD, Δ*tonB1*-PDD, and Δ*tonB2*-PDD are presented in Table 3. In the course of the 26 physiological and biochemical tests conducted, all three strains exhibited positive reactions in the glucose fermentation, rhamnose fermentation, urease, and Voges–Proskauer tests (separate commercial test systems). Conversely, negative outcomes were obtained for all the other tested characteristics under examination. These findings indicated that the deletion of *tonB1* or *tonB2* did not change the physiological and biochemical characteristics of PDD, implying that *tonB1* and *tonB2* are not directly associated with the conventional physiological and biochemical metabolic pathways of this bacterium.

Table 3. Differences in physiological and biochemical characteristics between WT-PDD and Δ*tonB1*/Δ*tonB2*-PDD.

Physiological and Biochemical Indicators	WT-PDD	Δ*tonB1*-PDD	Δ*tonB2*-PDD
Rhamnose fermentation	+	+	+
Amygdalin	-	-	-
Lactose (3% NaCl)	-	-	-
Lysine decarboxylase (3% NaCl)	-	-	-
Melibiose	-	-	-
Mannitol (3% NaCl)	-	-	-
Peptone water with 10% NaCl	-	-	-
Peptone water with 6% NaCl	-	-	-
Peptone water with 3% NaCl	-	-	-
Salt-free peptone water	-	-	-
Ornithine decarboxylase (3% NaCl)	-	-	-
Glucose (3% NaCl)	+	+	+
Inositol	-	-	-
Sucrose (3% NaCl)	-	-	-
Sorbitol fermentation	-	-	-
Xylose fermentation	-	-	-
Urease (3% NaCl)	+	+	+
Gelatin liquefaction (3% NaCl)	-	-	-
Arabitol (3% NaCl)	-	-	-
Voges–Proskauer test (3% NaCl MR-VP medium)	-	-	-
Malonate	-	-	-
Simmons citrate	-	-	-
H_2S production (3% NaCl)	-	-	-
Indole test (Kovacs reagent)	-	-	-
Voges–Proskauer test (separate commercial test system)	+	+	+
Oxidase test strip	-	-	-

Note: -: Negative, +: positive.

3.8. Differences in Antimicrobial Susceptibility

The antimicrobial susceptibility profiles of WT-PDD, Δ*tonB1*-PDD, and Δ*tonB2*-PDD are presented in Table 4. All three strains were categorized as either susceptible or intermediate to 29 antibiotics, including chloramphenicol, florfenicol, gentamicin, and kanamycin. In contrast, they were resistant to nine antibiotics, including penicillin, oxacillin, and streptomycin. No notable differences in antimicrobial susceptibility were detected among the three strains. These results indicated that the deletion of *tonB1* or *tonB2* did not significantly change the antibiotic susceptibility profile of PDD, suggesting that *tonB1* and *tonB2* are not directly associated with antibiotic metabolism or the mechanisms responsible for antimicrobial resistance in this bacterium.

Table 4. Differences in antibiotic susceptibility between WT-PDD and Δ*tonB1*/Δ*tonB2*-PDD.

No.	Antibiotics	Specification (μg/disc)	Strain		
			WT-PDD	Δ*tonB1*-PDD	Δ*tonB2*-PDD
1	Cephalexin	30	I	I	I
2	Cefazolin	30	S	S	S
3	Cefradine	30	S	S	S
4	Ceftazidime	30	S	S	S
5	Ceftriaxone	30	S	S	S
6	Cefotaxime	30/10	S	S	S
7	Ceftizoxime	30	S	S	S
8	Cefoperazone/Sulbactam	75/75	S	S	S
9	Penicillin	10	R	R	R
10	Oxacillin	1	R	R	R
11	Ampicillin	10	R	R	R
12	Amikacin	30	R	R	R
13	Gentamicin	10	I	I	I
14	Kanamycin	30	I	I	I
15	Streptomycin	10	R	R	R
16	Neomycin	30	R	R	R
17	Tetracycline	30	S	S	S
18	Doxycycline	30	S	S	S
19	Minocycline	30	S	S	S
20	Erythromycin	15	R	R	R
21	Acetylspiramycin	30	R	R	R
22	Clarithromycin	15	R	R	R
23	Azithromycin	15	I	I	I
24	Nalidixic acid	30	S	S	S
25	Pipemidic acid	30	S	S	S
26	Norfloxacin	10	S	S	S
27	Ofloxacin	5	S	S	S
28	Ciprofloxacin	5	S	S	S
29	Lomefloxacin	10	S	S	S
30	Fleroxacin	5	S	S	S
31	Polymyxin B	300IU	S	S	S
32	Novobiocin	30	S	S	S
33	Sulfisoxazole	300	S	S	S
34	Furazolidone	30	S	S	S
35	Rifampicin	5	S	S	S
36	Chloramphenicol	30	S	S	S
37	Enrofloxacin	10	S	S	S
38	Florfenicol	30	S	S	S

Note: R, resistant; I, intermediate; S, susceptible.

3.9. Comparison of Pathogenicity Between WT-PDD and ΔtonB1/ΔtonB2-PDD

As shown in Figure 9, the pathogenicity of WT-PDD, Δ*tonB1*-PDD, and Δ*tonB2*-PDD was compared in black rockfish (*S. schlegelii*) over an 8-day observation period with two challenge levels. At the high-dose level, WT-PDD resulted in the death of all 20 fish by day 2, with an actual dose of 1.21×10^8 CFU/mL. In comparison, by day 2, 17 out of 20 fish in the Δ*tonB1*-PDD group and 18 out of 20 fish in the Δ*tonB2*-PDD group had died, with actual doses of 1.32×10^8 and 1.24×10^8 CFU/mL, respectively. Both mutant groups ultimately reached 100% cumulative mortality by day 3. Kaplan–Meier survival curves did not show a significant difference among the three strains at the high-dose level (log-rank test, $\chi^2 = 2.094$, df = 2, $p = 0.351$). At the low-dose level, WT-PDD resulted in 12 out of 20 deaths by day 2 and 80% cumulative mortality by day 8, at an actual dose of 1.21×10^6 CFU/mL. Under similar low-dose challenge conditions, 12 out of 20 fish in the Δ*tonB1*-PDD group

had died by day 2, with cumulative mortality reaching 70% by day 8. Meanwhile, 13 out of 20 fish in the Δ*tonB2*-PDD group had died by day 2, with cumulative mortality reaching 80% by day 8. No significant difference was detected among the survival curves of the three groups at the low-dose level (log-rank test, $\chi^2 = 0.528$, df = 2, $p = 0.768$). Bonferroni-adjusted pairwise comparisons likewise showed no significant differences between strains at either challenge level (all adjusted $p \geq 0.440$). Overall, no significant differences were detected among the survival curves of the three challenge groups at either challenge dose.

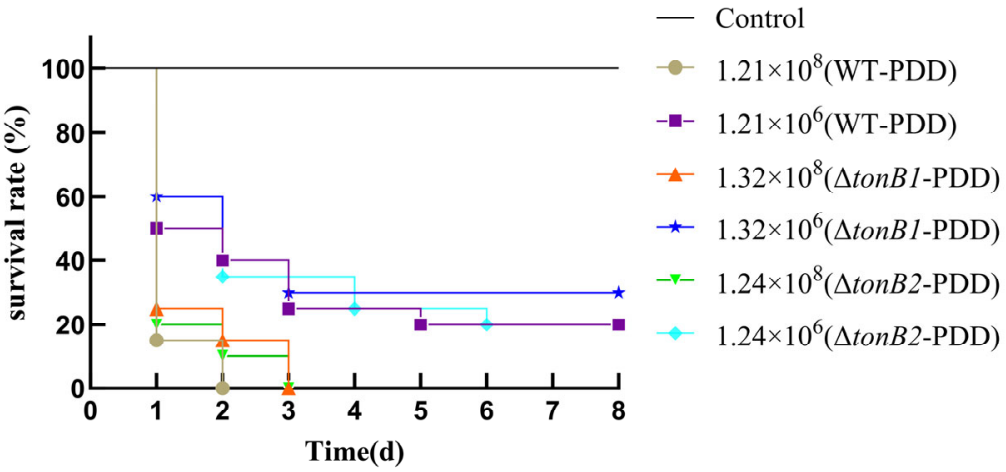

Figure 9. Results of the experimental infection assay using the wild-type strain WT-PDD and the Δ*tonB1*/Δ*tonB2*-PDD mutant strains. Kaplan–Meier curves were compared individually at each dose via the log-rank (Mantel–Cox) test. Neither the overall tests (higher dose, $p = 0.351$; lower dose, $p = 0.768$) nor Bonferroni-adjusted pairwise comparisons showed statistical significance ($n = 20$ per group).

4. Discussion

Both mutants maintained WT-like colony morphology on TSB, 2216E, TCBS, and iron-restricted LB agar. All strains exhibited comparable swarming zones, measuring 13 ± 0.76 mm. The physiological, biochemical, and antimicrobial susceptibility profiles remained unchanged. This is in contrast to the more extensive effects on morphology and motility reported for surface-associated regulatory systems in PDD [37]. In contrast, under iron limitation induced by 100 μM dip, the maximum bacterial density decreased from 4.51×10^8 CFU/mL in WT-PDD to 4.00×10^8 and 3.64×10^8 CFU/mL in Δ*tonB1*-PDD and Δ*tonB2*-PDD, respectively. Simultaneously, the intracellular iron content declined from $3.75 \times 10^{-4} \pm 4.00 \times 10^{-6}$ to $3.13 \times 10^{-4} \pm 1.05 \times 10^{-5}$ and $2.55 \times 10^{-4} \pm 2.00 \times 10^{-5}$ nmol/10^6 cells, respectively. Biofilm formation was also reduced, with OD_{595} values decreasing from 1.49 ± 0.10 to 1.16 ± 0.05 and 1.12 ± 0.04, respectively. This selective impairment of low-iron growth, iron accumulation, and biofilm formation is consistent with the established role of TonB-dependent systems in nutrient uptake and iron-associated transport [38,39]. These findings indicate that the TonB system is not essential for maintaining the basic cellular morphology or the typical physiological and biochemical characteristics of PDD. Given that antimicrobial susceptibility in Gram-negative bacteria is governed by multiple processes, including outer-membrane permeability, porin-mediated influx, efflux, target alteration, and enzymatic inactivation [40], the unchanged susceptibility profiles suggest that deletion of *tonB1* or *tonB2* did not broadly alter the antimicrobial-response processes assessed here. Instead, the TonB system is more likely involved in iron acquisition and iron-dependent adaptive processes, thereby contributing to the ability of PDD to respond to fluctuations in environmental iron availability.

The canonical function of the TonB system is to supply the energy needed for receptor-mediated transport of siderophores and heme across the outer membrane of Gram-negative bacteria. In this study, the deletion of *tonB1* or *tonB2* led to a decrease in intracellular iron levels and hindered growth under low-iron conditions. This finding is in line with the well-established role of the TonB system in iron acquisition among Gram-negative bacteria. Notably, the decrease in intracellular iron content and the growth defect under iron-limited conditions were more significant in Δ*tonB2*-PDD compared to Δ*tonB1*-PDD, indicating that *tonB2* might play a more crucial role in the iron acquisition system of PDD. This observation is consistent with previous findings in several bacterial pathogens, where multiple *tonB* homologs exhibit functional specialization and do not contribute equally to iron uptake. Mechanistically, TonB homologs may exhibit differences in the range of outer-membrane TonB-dependent receptors they energize. This is because receptor recognition depends on specific interactions involving the receptor-binding region of TonB. Differences in the coupling to ExbB-ExbD components may further influence their relative activities [3,4,19,20]. Given that *tonB1* and *tonB2* are located on different chromosomes in PDD, distinct regulatory contexts may also contribute to their unequal functional contributions. Correspondingly, the stronger phenotype of Δ*tonB2*-PDD suggests that the iron-acquisition pathways active under the present low-iron condition are more reliant on TonB2, whereas TonB1 provides a partially overlapping contribution. However, TonB protein abundance, TonB–receptor interactions, and substrate-specific transport were not directly examined in this study; therefore, this mechanistic interpretation awaits further testing. Comparison with TonB systems characterized in other fish pathogens indicates that the relative contributions of TonB homologs are dependent on both the substrate and the species. In *Vibrio anguillarum*, both TonB systems participate in iron transport. Specifically, TonB2 is essential for the uptake of ferric-anguibactin and makes the principal contribution to virulence in rainbow trout [38]. PDD exhibited a similar TonB2-biased phenotype under iron limitation. Deletion of either homolog led to a reduction in intracellular iron content and bacterial growth, yet these effects were more prominent in Δ*tonB2*-PDD. However, the significant phenotypes observed in both PDD mutants indicate partially overlapping functions under the tested conditions, rather than an exclusively TonB2-dependent pathway. A distinct pattern of functional specialization has been reported in *Vibrio alginolyticus*, where TonB1 specifically facilitates the utilization of hemin and hemoglobin, while both TonB systems contribute to the utilization of ferrichrome and vibrioferrin [41]. This contrast indicates that the relative importance of individual TonB homologs depends on the available iron source and the repertoire of cognate outer-membrane receptors. Because the present study imposed general iron limitation using 2,2′-dipyridyl rather than examining defined iron substrates, the stronger phenotype of Δ*tonB2*-PDD demonstrates a greater contribution of TonB2 under the tested low-iron condition. However, it does not confirm substrate specificity or the universal dominance of TonB2. The restriction of the PDD growth defects to low-iron conditions is consistent with the iron-dependent growth defects reported for *Edwardsiella ictaluri tonB* and *Flavobacterium psychrophilum exbD2* mutants [42,43]. Nevertheless, those mutations attenuated virulence in their respective fish hosts, whereas neither single *tonB* deletion in PDD significantly altered fish survival. Thus, in PDD, the measurable impairment of iron acquisition did not result in a detectable attenuation in the present intramuscular challenge model. This may be attributed to a partial functional overlap between TonB1 and TonB2, compensation by alternative iron-uptake pathways, or differences among the experimental infection models. Furthermore, under conditions of exogenous iron supplementation, the growth of the two deletion mutants was not further impaired; rather, their growth slightly exceeded that of the wild-type strain. A more reasonable explanation is that elevated extracellular iron levels may partly cir-

cumvent the need for TonB-dependent high-affinity iron uptake or relieve the metabolic burden associated with maintaining iron acquisition stress responses. Therefore, these findings should not be regarded as evidence that the deletion of *tonB* itself has a growth-promoting effect. Considering the previously reported heme utilization system, citrate-mediated iron transport strategy, and other potential iron acquisition pathways in PDD, this bacterium probably has a strong and multifaceted ability to compensate for iron acquisition via alternative routes.

Consistent with the iron acquisition phenotypes observed in this study, the transcriptional data indicated different expression patterns subsequent to the deletion of *tonB1* and *tonB2* in PDD. Overall, the expression levels of the analyzed genes remained relatively stable in Δ*tonB1*-PDD. In contrast, Δ*tonB2*-PDD exhibited modest (<2-fold) but statistically significant changes in the expression of several genes. Specifically, *hutZ*, *fur*, $hlyA_{pl}$, $hlyA_{ch}$, *plpV*, *lapB*, *dly*, *tonB1*, and *cheY* were all upregulated to varying degrees. Given the established interplay between iron homeostasis and Fur-mediated virulence regulation [44], these findings suggest that the deletion of *tonB2* was associated with modest transcriptional adjustments involving genes related to iron homeostasis, cell-envelope homeostasis, and virulence regulation. Collectively, these observations suggest that the deletion of *tonB2* might affect the transcriptional responses related to iron homeostasis and the utilization of iron sources in PDD [45]. However, the transcriptional changes detected in this study were not accompanied by corresponding enhancements in hemolytic activity or phospholipase activity [46]. This finding indicates that up-regulation of virulence-associated genes at the transcriptional level does not necessarily lead to an increase in the production of secreted proteins or an enhancement of extracellular enzymatic activity [47]. The virulence output of PDD is regulated at multiple levels, which involves not only transcriptional regulation but also the efficiency of secretion systems, environmental osmolarity, and host-derived signals [48]. Although changes in less than twofold may be biologically relevant in some regulatory contexts, statistical significance alone does not confirm functional importance. Therefore, the up-regulation of virulence-associated transcripts observed in Δ*tonB2*-PDD should be interpreted as a transcription-level association whose biological significance remains undetermined, rather than direct evidence of enhanced virulence.

Although deletion of *tonB1* or *tonB2* impaired iron acquisition, growth under iron-limited conditions, and biofilm formation, Kaplan–Meier analysis detected no significant differences among the survival curves of WT-PDD, Δ*tonB1*-PDD, and Δ*tonB2*-PDD at either challenge dose. At the higher dose, both mutants reached 100% mortality one day later than WT-PDD; however, this numerical difference was not statistically significant and should not be interpreted as evidence of attenuated pathogenicity. The absence of a detectable survival difference may reflect the multifactorial nature of pathogenicity in fish-pathogenic *Vibrionaceae*, in which iron acquisition represents only one of several determinants of in vivo fitness and disease progression [49]. Several factors may have limited the ability of the present model to resolve more subtle contributions of individual TonB homologs. First, PDD has multiple iron acquisition pathways, and the loss of a single *tonB* homolog may be partly compensated by alternative uptake systems. Second, the intramuscular challenge model, especially at high bacterial doses, is more appropriate for evaluating acute virulence than for detecting subtle differences in early adhesion, colonization, or nutrient competition. Third, the acute lethality of PDD is strongly associated with hemolysins and other secreted virulence factors. Consistently, the deletion of the T2SS core gene *gspD* was previously shown to impair hemolytic and phospholipase activities and reduce PDD pathogenicity [50]. Therefore, *tonB1* and *tonB2* appear to be involved in iron-dependent adaptation and host–pathogen interactions, but they are unlikely to be the sole determinants of acute lethal virulence in PDD. The diminished biofilm formation

further suggests that TonB-dependent iron acquisition plays a role in biofilm development in PDD. Both Δ*tonB1*-PDD and Δ*tonB2*-PDD produced significantly less biofilm biomass compared to WT-PDD, which indicates that the loss of either *tonB* homolog impairs this surface-associated adaptive characteristic. Active iron uptake and intracellular iron availability have been shown to serve as signals for biofilm maturation through Fur-dependent regulation. In *Pseudomonas aeruginosa*, the disruption of high-affinity iron uptake resulted in defective biofilm development. In contrast, the delivery of iron through an alternative uptake pathway restored the formation of structured biofilm [51]. In *Vibrio cholerae*, Fur directly regulates genes associated with c-di-GMP turnover and exopolysaccharide biosynthesis, which demonstrate a regulatory link between iron homeostasis and biofilm matrix production. The direction and iron dependence of this regulation may vary among bacterial species [52]. Thus, the impairment of TonB-dependent iron acquisition in PDD may disrupt intracellular iron sensing and downstream matrix-production pathways, thereby contributing to the reduced biofilm biomass observed in both mutants. However, intracellular iron during the biofilm assay, Fur activity, c-di-GMP levels, and biofilm matrix gene expression were not examined; therefore, this proposed mechanism needs to be tested in PDD. Since biofilms are generally associated with surface attachment, environmental persistence, and tolerance to nutrient limitation, the biofilm deficiency observed here might be relevant to PDD survival under environmental or host-associated conditions that are not completely represented by the acute intramuscular challenge model. Although no significant survival differences were detected in the acute intramuscular challenge assay, TonB-dependent iron acquisition may still contribute to surface persistence and colonization-related processes that are not fully represented by this model. This possibility requires direct evaluation in future studies.

As a highly hemolytic pathogen that frequently leads to skin ulceration and hemorrhagic symptoms in its hosts, the iron acquisition system of PDD requires further exploration based on the findings of the current study. Firstly, in this work, only single-gene deletion mutants of *tonB1* and *tonB2* were examined, and the potential for functional complementation between these two homologs cannot be entirely ruled out. The construction of a double-deletion mutant, along with comprehensive in vitro and in vivo phenotypic characterization, would provide a more comprehensive understanding of the overall contribution of the TonB system to the physiology, growth, and pathogenicity of PDD. Secondly, the current study did not distinguish the utilization preferences of different iron sources, and thus it was unable to determine whether TonB1 and TonB2 preferentially function in the transport of specific substrates or interact with distinct outer membrane receptors. Future studies should investigate the utilization of various iron sources, such as heme, hemoglobin, ferric citrate, and potential siderophores, via more precise substrate-specific assays.

5. Conclusions

In this study, single-deletion mutants of *tonB1* and *tonB2* and their corresponding complemented strains were constructed in *Photobacterium damselae* subsp. *damselae*. Deletion of either gene impaired growth and intracellular iron accumulation under iron-limited conditions, and these defects were largely restored by complementation, indicating that both *tonB1* and *tonB2* contribute to iron acquisition and low-iron adaptation. The effects were more pronounced in Δ*tonB2*-PDD. Modest transcriptional changes in several iron uptake- and virulence-associated genes were also detected in Δ*tonB2*-PDD, although their biological significance remains unresolved. Both mutants showed reduced biofilm formation, whereas colony morphology, swarming motility, hemolytic and phospholipase activities, physiological and biochemical traits, and antimicrobial susceptibility were largely

unchanged. In the black rockfish intramuscular challenge model, Kaplan–Meier analysis detected no significant differences among the survival curves of WT-PDD, Δ*tonB1*-PDD, and Δ*tonB2*-PDD at either challenge dose. Taken together, these results indicate that *tonB1* and *tonB2* contribute to iron-dependent adaptation and biofilm formation in PDD; however, no significant difference in fish survival was detected between WT-PDD and either single-gene deletion mutant under the present challenge conditions.

Author Contributions: Y.J.: Data Curation, Validation, Formal Analysis, Methodology, Writing. H.J.: Supervision, Validation, Formal Analysis, Writing—Review & Editing. Z.Z (Zhiqi Zhang).: Funding Acquisition, Methodology. Y.Y.: Funding Acquisition, Investigation, Methodology, Software. C.W.: Funding Acquisition, Methodology, Formal Analysis. Y.W.: Methodology, Resources, Formal Analysis. X.R.: Funding Acquisition, Investigation, Methodology, Software. A.M.: Data Curation, Software. S.L.: Resources. Z.Z (Zheng Zhang).: Conceptualization, Writing—Review & Editing, Methodology, Software. All authors have read and agreed to the published version of the manuscript.

Funding: This research was funded by the Natural Science Foundation of Shandong Province (ZR2025QC229 and ZR2026MS0469); the China Postdoctoral Science Foundation (2025M773138); the Hebei Provincial High-level Talent Program (2023HBQZYCSB019); and the Central Public-interest Scientific Institution Basal Research Fund (2023TD29).

Institutional Review Board Statement: This study was conducted in accordance with the standard procedures for the care and use of laboratory animals in China and approved by the Animal Ethics Committee of the Yellow Sea Fisheries Research Institute, Chinese Academy of Fishery Sciences (Approval code: YSFRI-2025062 and approval date: 16 May 2025).

Data Availability Statement: The original contributions presented in this study are included in the article. Further inquiries can be directed to the corresponding author.

Conflicts of Interest: Author Shuyi Li was employed by the company Huanghua Jinhui Aquatic Products Breeding and Development. The remaining authors declare that the research was conducted in the absence of any commercial or financial relationships that could be construed as a potential conflict of interest.

References

1. Cassat, J.E.; Skaar, E.P. Iron in infection and immunity. *Cell Host Microbe* **2013**, *13*, 509–519. [CrossRef] [PubMed]
2. Murdoch, C.C.; Skaar, E.P. Nutritional immunity: The battle for nutrient metals at the host–pathogen interface. *Nat. Rev. Microbiol.* **2022**, *20*, 657–670. [CrossRef] [PubMed]
3. Noinaj, N.; Guillier, M.; Barnard, T.J.; Buchanan, S.K. TonB-dependent transporters: Regulation, structure, and function. *Annu. Rev. Microbiol.* **2010**, *64*, 43–60. [CrossRef] [PubMed]
4. Silale, A.; van den Berg, B. TonB-dependent transport across the bacterial outer membrane. *Annu. Rev. Microbiol.* **2023**, *77*, 67–88. [CrossRef] [PubMed]
5. Holden, K.M.; Browning, G.F.; Noormohammadi, A.H.; Markham, P.F.; Marenda, M.S. TonB is essential for virulence in avian pathogenic *Escherichia coli*. *Comp. Immunol. Microbiol. Infect. Dis.* **2012**, *35*, 129–138. [CrossRef] [PubMed]
6. Lemos, M.L.; Balado, M. Iron uptake mechanisms as key virulence factors in bacterial fish pathogens. *J. Appl. Microbiol.* **2020**, *129*, 104–115. [CrossRef] [PubMed]
7. Gouife, M.; Chen, S.; Huang, K.; Nawaz, M.; Jin, S.; Ma, R.; Wang, Y.; Xue, L.; Xie, J. *Photobacterium damselae* subsp. *damselae* in mariculture. *Aquac. Int.* **2022**, *30*, 1453–1480. [CrossRef]
8. Rivas, A.J.; Lemos, M.L.; Osorio, C.R. *Photobacterium damselae* subsp. *damselae*, a bacterium pathogenic for marine animals and humans. *Front. Microbiol.* **2013**, *4*, 283. [CrossRef] [PubMed]
9. Osorio, C.R.; Vences, A.; Matanza, X.M.; Terceti, M.S. *Photobacterium damselae* subsp. *damselae*, a generalist pathogen with unique virulence factors and high genetic diversity. *J. Bacteriol.* **2018**, *200*, e00002-18. [CrossRef] [PubMed]
10. Rivas, A.J.; Balado, M.; Lemos, M.L.; Osorio, C.R. The *Photobacterium damselae* subsp. *damselae* hemolysins damselysin and HlyA are encoded within a new virulence plasmid. *Infect. Immun.* **2011**, *79*, 4617–4627. [CrossRef] [PubMed]

11. Vences, A.; Rivas, A.J.; Lemos, M.L.; Husmann, M.; Osorio, C.R. Chromosome-encoded hemolysin, phospholipase, and collagenase in plasmidless isolates of *Photobacterium damselae* subsp. *damselae* contribute to virulence for fish. *Appl. Environ. Microbiol.* **2017**, *83*, e00401-17. [CrossRef] [PubMed]
12. Wang, Z.; Shi, C.; Wang, H.; Wan, X.; Zhang, Q.; Song, X.; Li, G.; Gong, M.; Ye, S.; Xie, G.; et al. A novel research on isolation and characterization of *Photobacterium damselae* subsp. *damselae* from Pacific white shrimp, *Penaeus vannamei*, displaying black gill disease cultured in China. *J. Fish. Dis.* **2020**, *43*, 551–559. [CrossRef] [PubMed]
13. Río, S.J.; Osorio, C.R.; Lemos, M.L. Heme uptake genes in human and fish isolates of *Photobacterium damselae*: Existence of *hutA* pseudogenes. *Arch. Microbiol.* **2005**, *183*, 347–358. [CrossRef] [PubMed]
14. Balado, M.; Puentes, B.; Couceiro, L.; Fuentes-Monteverde, J.C.; Rodríguez, J.; Osorio, C.R.; Jiménez, C.; Lemos, M.L. Secreted citrate serves as iron carrier for the marine pathogen *Photobacterium damselae* subsp. *damselae*. *Front. Cell. Infect. Microbiol.* **2017**, *7*, 361. [CrossRef] [PubMed]
15. Puentes, B.; Souto, A.; Balado, M.; Rodríguez, J.; Osorio, C.R.; Jiménez, C.; Lemos, M.L. A novel genomic island encodes vibrioferrin synthesis in the marine pathogen *Photobacterium damselae* subsp. *damselae*. *Microb. Pathog.* **2025**, *199*, 107218. [CrossRef] [PubMed]
16. Yamamoto, S.; Okujo, N.; Yoshida, T.; Matsuura, S.; Shinoda, S. Structure and iron transport activity of vibrioferrin, a new siderophore of *Vibrio parahaemolyticus*. *J. Biochem.* **1994**, *115*, 868–874. [CrossRef] [PubMed]
17. Barca, A.V.; Vences, A.; Terceti, M.S.; Vale, A.D.; Osorio, C.R. Low salinity activates a virulence program in the generalist marine pathogen *Photobacterium damselae* subsp. *damselae*. *mSystems* **2023**, *8*, e01253-22. [CrossRef] [PubMed]
18. Matanza, X.M.; Osorio, C.R. Exposure of the opportunistic marine pathogen *Photobacterium damselae* subsp. *damselae* to human body temperature is a stressful condition that shapes the transcriptome, viability, cell morphology, and virulence. *Front. Microbiol.* **2020**, *11*, 1771. [CrossRef] [PubMed]
19. Liao, H.B.; Cheng, X.; Zhu, D.K.; Wang, M.; Jia, R.; Chen, S.; Chen, X.; Biville, F.; Liu, M.; Cheng, A. TonB energy transduction systems of *Riemerella anatipestifer* are required for iron and hemin utilization. *PLoS ONE* **2015**, *10*, e0127506. [CrossRef] [PubMed]
20. Zimbler, D.L.; Arivett, B.A.; Beckett, A.C.; Menke, S.M.; Actis, L.A. Functional features of TonB energy transduction systems of *Acinetobacter baumannii*. *Infect. Immun.* **2013**, *81*, 3382–3394. [CrossRef] [PubMed]
21. Runci, F.; Gentile, V.; Frangipani, E.; Rampioni, G.; Leoni, L.; Lucidi, M.; Visaggio, D.; Harris, G.; Chen, W.; Stahl, J.; et al. Contribution of active iron uptake to *Acinetobacter baumannii* pathogenicity. *Infect. Immun.* **2019**, *87*, e00755-18. [CrossRef] [PubMed]
22. Naka, H.; Hirono, I.; Aoki, T. Cloning and characterization of two types of *tonB* genes, *tonB1* and *tonB2*, and ferric uptake regulator gene, *fur*, from *Photobacterium damselae* subsp. *piscicida*. *Fish Pathol.* **2005**, *40*, 73–79. [CrossRef]
23. Lu, F.; Miao, S.; Tu, J.; Ni, X.; Xing, L.; Yu, H.; Pan, L.; Hu, Q. The role of TonB-dependent receptor TbdR1 in *Riemerella anatipestifer* in iron acquisition and virulence. *Vet. Microbiol.* **2013**, *167*, 713–718. [CrossRef] [PubMed]
24. Zhang, Z.; Yu, Y.; Chen, J.; Wang, Y.; Jiang, Y.; Liao, M.; Rong, X.; Zhang, H. Development of a microfluidics-based quantitative real-time PCR to rapidly identify *Photobacterium damselae* subsp. *damselae* with different pathogenicity by detecting the presence of mcp or dly gene. *J. Ocean Univ. China* **2021**, *20*, 445–453. [CrossRef]
25. Edwards, R.A.; Keller, L.H.; Schifferli, D.M. Improved allelic exchange vectors and their use to analyze 987P fimbria gene expression. *Gene* **1998**, *207*, 149–157. [CrossRef] [PubMed]
26. Simon, R.; Priefer, U.; Pühler, A. A broad host range mobilization system for in vivo genetic engineering: Transposon mutagenesis in Gram-negative bacteria. *Bio/Technology* **1983**, *1*, 784–791. [CrossRef]
27. Parales, R.E.; Harwood, C.S. Construction and use of a new broad-host-range *lacZ* transcriptional fusion vector, pHRP309, for Gram-negative bacteria. *Gene* **1993**, *133*, 23–30. [CrossRef] [PubMed]
28. Thode, S.K.; Kahlke, T.; Robertsen, E.M.; Hansen, H.; Haugen, P. The immediate global responses of *Aliivibrio salmonicida* to iron limitations. *BMC Microbiol.* **2015**, *15*, 9. [CrossRef] [PubMed]
29. Lages, M.A.; Ageitos, L.; Rodríguez, J.; Jiménez, C.; Lemos, M.L.; Balado, M. Identification of key functions required for production and utilization of the siderophore piscibactin encoded by the high-pathogenicity island irp-HPI in *Vibrionaceae*. *Int. J. Mol. Sci.* **2022**, *23*, 8865. [CrossRef] [PubMed]
30. Balado, M.; Lages, M.A.; Fuentes-Monteverde, J.C.; Martínez-Matamoros, D.; Rodríguez, J.; Jiménez, C.; Lemos, M.L. The siderophore piscibactin is a relevant virulence factor for *Vibrio anguillarum* favored at low temperatures. *Front. Microbiol.* **2018**, *9*, 1766. [CrossRef] [PubMed]
31. Livak, K.J.; Schmittgen, T.D. Analysis of relative gene expression data using real-time quantitative PCR and the $2^{-\Delta\Delta CT}$ method. *Methods* **2001**, *25*, 402–408. [CrossRef] [PubMed]
32. O'Toole, G.A. Microtiter dish biofilm formation assay. *J. Vis. Exp.* **2011**, *47*, e2437. [CrossRef] [PubMed]
33. Stepanović, S.; Vuković, D.; Holá, V.; Bonaventura, G.D.; Djukić, S.; Ćirković, I.; Ruzicka, F. Quantification of biofilm in microtiter plates: Overview of testing conditions and practical recommendations for assessment of biofilm production by staphylococci. *APMIS* **2007**, *115*, 891–899. [CrossRef] [PubMed]

34. CLSI. *Methods for Antimicrobial Broth Dilution and Disk Diffusion Susceptibility Testing of Bacteria Isolated from Aquatic Animals*, 2nd ed.; CLSI Guideline VET03; Clinical and Laboratory Standards Institute: Wayne, PA, USA, 2020.
35. Rivas, A.J.; Balado, M.; Lemos, M.L.; Osorio, C.R. Synergistic and additive effects of chromosomal and plasmid-encoded hemolysins contribute to hemolysis and virulence in *Photobacterium damselae* subsp. *damselae*. *Infect. Immun.* **2013**, *81*, 3287–3299. [CrossRef] [PubMed]
36. Eng, T.; Herbert, R.A.; Martinez, U.; Wang, B.; Chen, J.C.; Brown, J.B.; Deutschbauer, A.M.; Bissell, M.J.; Mortimer, J.C.; Mukhopadhyay, A. Iron supplementation eliminates antagonistic interactions between root-associated bacteria. *Front. Microbiol.* **2020**, *11*, 1742. [CrossRef] [PubMed]
37. Terceti, M.S.; Vences, A.; Matanza, X.M.; Barca, A.V.; Noia, M.; Lisboa, J.; dos Santos, N.M.S.; Vale, A.D.; Osorio, C.R. The RstAB system impacts virulence, motility, cell morphology, penicillin tolerance and production of type II secretion system-dependent factors in the fish and human pathogen *Photobacterium damselae* subsp. *damselae*. *Front. Microbiol.* **2019**, *10*, 897. [CrossRef] [PubMed]
38. Stork, M.; Di Lorenzo, M.; Mouriño, S.; Osorio, C.R.; Lemos, M.L.; Crosa, J.H. Two TonB systems function in iron transport in *Vibrio anguillarum*, but only one is essential for virulence. *Infect. Immun.* **2004**, *72*, 7326–7329. [CrossRef] [PubMed]
39. Krewulak, K.D.; Vogel, H.J. TonB or not TonB: Is that the question? *Biochem. Cell Biol.* **2011**, *89*, 87–97. [CrossRef] [PubMed]
40. Pagès, J.-M.; James, C.E.; Winterhalter, M. The porin and the permeating antibiotic: A selective diffusion barrier in Gram-negative bacteria. *Nat. Rev. Microbiol.* **2008**, *6*, 893–903. [CrossRef] [PubMed]
41. Wang, Q.; Liu, Q.; Cao, X.; Yang, M.; Zhang, Y. Characterization of two TonB systems in marine fish pathogen *Vibrio alginolyticus*: Their roles in iron utilization and virulence. *Arch. Microbiol.* **2008**, *190*, 595–603. [CrossRef] [PubMed]
42. Abdelhamed, H.; Lawrence, M.L.; Karsi, A. The role of TonB gene in *Edwardsiella ictaluri* virulence. *Front. Physiol.* **2017**, *8*, 1066. [CrossRef] [PubMed]
43. Álvarez, B.; Álvarez, J.; Menéndez, A.; Guijarro, J.A. A mutant in one of two *exbD* loci of a TonB system in *Flavobacterium psychrophilum* shows attenuated virulence and confers protection against cold water disease. *Microbiology* **2008**, *154*, 1144–1151. [CrossRef] [PubMed]
44. Porcheron, G.; Dozois, C.M. Interplay between iron homeostasis and virulence: Fur and RyhB as major regulators of bacterial pathogenicity. *Vet. Microbiol.* **2015**, *179*, 2–14. [CrossRef] [PubMed]
45. Puentes, B.; Balado, M.; Bermúdez-Crespo, J.; Osorio, C.R.; Lemos, M.L. A proteomic analysis of the iron response of *Photobacterium damselae* subsp. *damselae* reveals metabolic adaptations to iron level changes and novel potential virulence factors. *Vet. Microbiol.* **2017**, *201*, 257–264. [CrossRef] [PubMed]
46. Rivas, A.J.; Vences, A.; Husmann, M.; Lemos, M.L.; Osorio, C.R. *Photobacterium damselae* subsp. *damselae* major virulence factors Dly, plasmid-encoded HlyA, and chromosome-encoded HlyA are secreted via the type II secretion system. *Infect. Immun.* **2015**, *83*, 1246–1256. [CrossRef] [PubMed]
47. Liu, Y.; Beyer, A.; Aebersold, R. On the dependency of cellular protein levels on mRNA abundance. *Cell* **2016**, *165*, 535–550. [CrossRef] [PubMed]
48. Terceti, M.S.; Rivas, A.J.; Álvarez, L.; Noia, M.; Cava, F.; Osorio, C.R. *rstB* regulates expression of the *Photobacterium damselae* subsp. *damselae* major virulence factors damselysin, phobalysin P and phobalysin C. *Front. Microbiol.* **2017**, *8*, 582. [CrossRef] [PubMed]
49. Hickey, M.E.; Lee, J.L. A comprehensive review of *Vibrio (Listonella) anguillarum*: Ecology, pathology and prevention. *Rev. Aquac.* **2018**, *10*, 585–610. [CrossRef]
50. Liu, H.Z.; Yu, Y.X.; Wang, C.Y.; Wang, Y.; Wu, R.; Zhang, Z.; Liu, D.; Liao, M.; Rong, X.; Li, B.; et al. The molecular mechanism of *gspD* gene in regulating the biological characteristics, pathogenicity and virulence gene expression of *Photobacterium damselae* subsp. *damselae*. *Int. J. Biol. Macromol.* **2025**, *306*, 141559. [CrossRef] [PubMed]
51. Banin, E.; Vasil, M.L.; Greenberg, E.P. Iron and *Pseudomonas aeruginosa* biofilm formation. *Proc. Natl. Acad. Sci. USA* **2005**, *102*, 11076–11081. [CrossRef] [PubMed]
52. Gao, H.; Ma, L.; Qin, Q.; Qiu, Y.; Zhang, J.; Li, J.; Lou, J.; Diao, B.; Zhao, H.; Shi, Q.; et al. Fur represses *Vibrio cholerae* biofilm formation via direct regulation of *vieSAB*, *cdgD*, *vpsU*, and *vpsA-K* transcription. *Front. Microbiol.* **2020**, *11*, 587159. [CrossRef] [PubMed]